RSC Advances

PAPER

View Article Online
View Journal | View Issue

Cite this: *RSC Adv.*, 2018, **8**, 20056

Synthesis of gold nanorod/neodymium oxide yolk/shell composite with plasmon-enhanced near-infrared luminescence†

Yafang Zhang,*[ab] Jiahong Wang,*[bcd] Fan Nan[be] and Qu-Quan Wang*[b]

Received 12th February 2018
Accepted 17th May 2018

DOI: 10.1039/c8ra01342j

rsc.li/rsc-advances

A yolk/shell composite consisting of an AuNR core and an Nd_2O_3 shell with a 19 nm gap is synthesized by a multi-step over-growth method. The near-infrared luminescence of AuNR@Nd_2O_3 is up to 4.6 times higher than that of Nd_2O_3 hollow nanoparticles. The underlying mechanism of plasmon-induced luminescence enhancement is further investigated.

Rare earth (RE)-based nanostructures have attracted a lot of attention for their promising applications ranging from photonics to biomedicines.[1–4] The RE-based nanostructures have shown many advantages over the conventional luminescent materials such as semiconductor quantum dots (QDs) and organic dyes, as the luminescence of RE shows high purity, large stock-shifts and excellent stability.[5–7] On the other hand, the RE material is also bio-compatible, which suggests that it has great potential in bio-imaging and therapy.[8–10] Among the lanthanide elements, neodymium (Nd) has drawn a lot of interest for its potentials in sub-tissue imaging and bio-sensing as its luminescence is in the first biological window.[4,11,12] However, the absorption cross-section of Nd is smaller than those of semiconductors or dyes, which seriously affects its fluorescence efficiency, and this prevents its practical applications.[13,14]

Great efforts are being made to improve the fluorescence of RE,[15–17] in particular the combination between plasmonic noble metal structures and RE is an efficient approach.[18–20] When the light excites noble metal nanostructures, the electron gas collectively oscillates and generates plasmons near the metal surface.[21,22] The large absorption cross-section and strong local electromagnetic field dramatically improve the fluorescence efficiency of the nearby emitters.[23–25] Thus, various hybrids composed of RE nanoparticles and metal nanostructures are designed.[26–31] For instance, J. R. Lakowicz *et al.* encapsulated lanthanides with silver nanoshells, and the emissions were significantly enhanced by about 10 times.[26] For the case of Ag@SiO_2@Y_2O_3:Er synthesized by F. Zhang *et al.*, the up-conversion luminescence (UCL) of Y_2O_3:Er was enhanced 4 times by the inner Ag nanoparticles.[27] A. Priyam *et al.*[28] found that the fluorescence of $NaYF_4$:Yb, Er NPs can be improved by a gold-shell. The metal- and particle-size-dependent enhancements are both investigated.[29,30] In addition, various 3D metamaterials and photonic crystals have been designed to adjust or enhance the emissions of RE.[31]

The luminescence of RE can be improved by the coupled plasmons, because the plasmons provide strong electromagnetic field to enhance the excitation/emission process; also, there may be energy transfer between the plasmons and emitters.[32,33] Gold nanorod (AuNR) is a typical plasmonic structure used to enhance the fluorescence of emitters, and it has tunable longitudinal surface plasmon resonance (LSPR) ranging from visible to near-infrared.[34–36] Since the excitation and emission frequencies of Nd are both in the near-infrared region, it is possible to design a resonance structure between the AuNR and Nd structures to achieve luminescence enhancement of Nd^{3+}.[37] For obtaining luminescence enhancement, isolation between the plasmonic structure and the emitters is very important; silica, alumina, polymers, or DNAs have been applied to adjust the distance to obtain the largest enhancement.[27,38,39] However, there are a few reports on the structure consisting of a plasmonic core and an RE shell with a natural isolation layer; the plasmon-induced RE down-conversion luminescence enhancement is also not a popular topic.[40–42] In this study, we developed a facile method to prepare AuNR@Nd_2O_3 yolk/shell composites containing a 19 nm gap between an AuNR core and an Nd_2O_3 shell. The effects of AuNRs on the down-conversion luminescence (DCL) properties of Nd_2O_3 shells were studied by comparing the luminescence intensities of the AuNR@Nd_2O_3

[a]*School of Physics and Technology, University of Jinan, Jinan, 250022, P. R. China. E-mail: yfzhang_opt@126.com*

[b]*School of Physics and Technology, Wuhan University, Wuhan, 430072, P. R. China. E-mail: qqwang@whu.edu.cn*

[c]*Shenzhen Institutes of Advanced Technology, Chinese Academy of Sciences, Shenzhen 518055, P. R. China. E-mail: jh.wang1@siat.ac.cn*

[d]*Department of Physics, City University of Hong Kong, Kowloon, Hong Kong, P. R. China*

[e]*Department of Chemical and Biomolecular Engineering, Clarkson University, Potsdam, NY 13699, USA*

† Electronic supplementary information (ESI) available: Synthesis of gold nanorod/neodymium oxide yolk/shell composite with plasmon enhanced near-infrared luminescence. See DOI: 10.1039/c8ra01342j

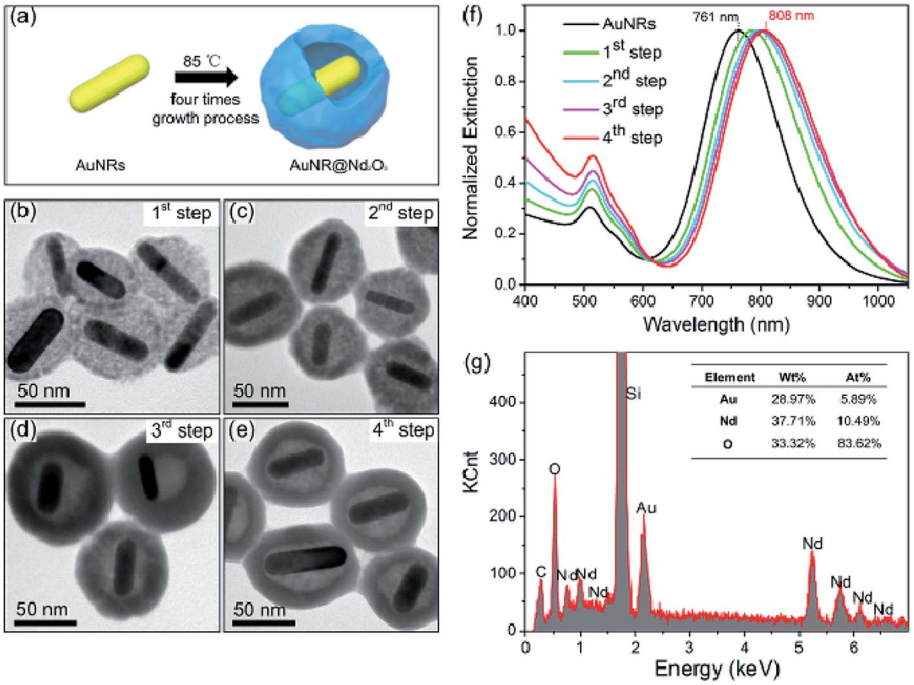

Fig. 1 (a) Schematic illustration of the growth procedure of the AuNR@Nd_2O_3 yolk/shell composites. (b–e) TEM images of AuNR@Nd_2O_3 composites obtained at different growth steps. (f) Normalized extinction spectra of AuNRs and AuNR@Nd_2O_3 composites obtained at different growth steps. (g) EDX spectrum of the final AuNR@Nd_2O_3 yolk/shell composites.

yolk/shell composites and the corresponding Nd_2O_3 hollow nanoparticles. It was found that the 873 nm emission of Nd^{3+} was enhanced by AuNRs up to 4.6 times. The LSPR-dependent enhancement was also investigated further.

Cetyl-trimethyl ammonium bromide (CTAB)-capped AuNRs were first synthesized using the seed-mediated growth method.[43,44] Then, CTAB was replaced by oleate with a ligand exchange approach.[42] Au@Nd_2O_3 yolk/shell composites were

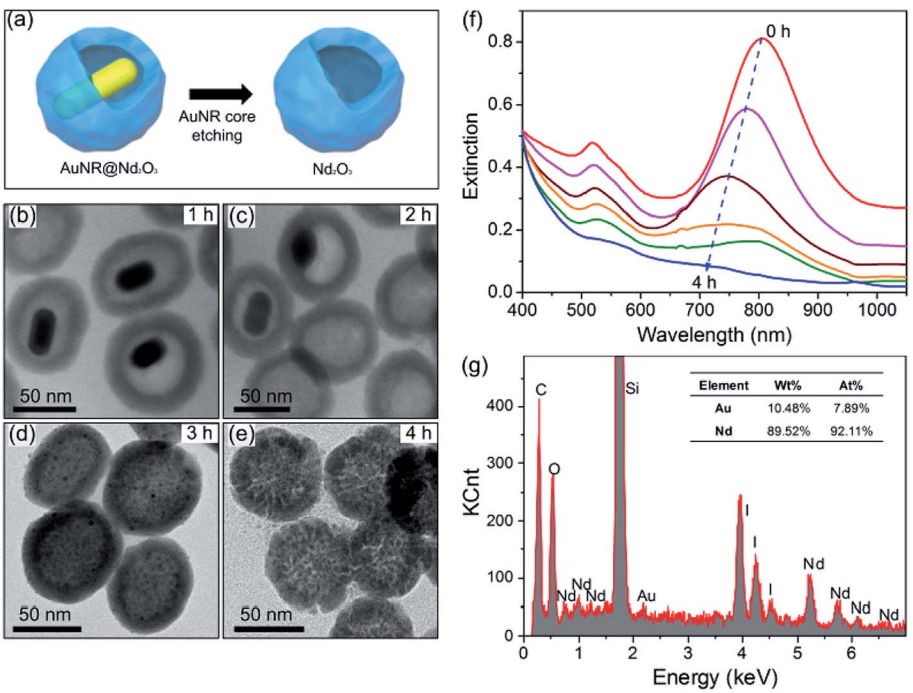

Fig. 2 (a) Schematic illustration of the etching formation process of the Nd_2O_3 hollow nanoparticles. (b–e) TEM images of the as-synthesised AuNR@Nd_2O_3 nanocomposites after (b) 1 h, (c) 2 h, (d) 3 h and (e) 4 h of etching. (f) Time evolution of the extinction spectra during the etching process. (g) EDX spectrum of the Nd_2O_3 hollow nanoparticles.

prepared by an oleate-assisted hydrothermal method. In brief, for the 1st step of the growth procedure, 5 mL aqueous solution of oleate-AuNRs was diluted with 14 mL of ultrapure water. $Nd(NO_3)_3$ and HMT solutions were injected with stirring to form a well-dispersed solution; the mixture was incubated at 85 °C for 3 h, in which $Nd(NO_3)_3$ and HMT served as the cation and anion reagents, respectively. Then, the resultant solution was centrifuged; the precipitate was re-dispersed in ultrapure water, and it was used as seeds in the next step. This process was repeated three times to achieve the final yolk/shell composites (Fig. 1(a)). The transmission electron microscopy (TEM) images in Fig. 1(b–e) indicate the morphology evolution in the whole growth process. The length and diameter of the original AuNRs were about 60 nm and 15 nm, respectively, thus suggesting an aspect ratio of 4 (Fig. ESI-1a†). After the 3 hour 1st step growth, the Nd_2O_3 nanoparticles loosely surrounded AuNRs (Fig. 1(b)). In the 2nd growth step, the outer Nd_2O_3 shell became thicker and more compact (Fig. 1(c)). A gap formed between the AuNR core and the Nd_2O_3 shell, and the thickness of the Nd_2O_3 shell decreased from 28 nm to 16 nm after the 3rd growth step (Fig. 1(d)), which was probably due to the Ostwald ripening.[45,46] When the 4th growth step was completed, the final products were collected. Fig. 1(e) and Fig. ESI-1b† demonstrate that the as-prepared hybrids were monodispersed hollow quasi-spheres consisting of AuNR cores and Nd_2O_3 shells. Interestingly, AuNRs were completely separated from Nd_2O_3, and the gap was about 19 nm. During the growth process, LSPR of AuNRs gradually red-shifted from 761 nm to 808 nm as the surrounding Nd_2O_3 increased the refractive index (Fig. 1(f)).[47] The energy-dispersive X-ray (EDX) spectrum in Fig. 1(g) displays the relative element contents of the final AuNR@Nd_2O_3 composites; the Au/Nd ratio was about 4 : 6.

To reveal the plasmonic effect on the luminescence of Nd_2O_3, iodide/triiodide redox couple is used to corrode the inner AuNRs and to achieve the Nd_2O_3 hollow nanoparticles (Fig. 2(a)). Fig. 2(b–e) show the morphology evolution against the etching time. After etching for 1 h, AuNRs decrease in size and after 2 h, they transform into quasi-spheres about 10 nm in diameter. Then, AuNRs transform into 2–3 nm spheres after 3 h and finally disappear after 4 h. The completely etched Nd_2O_3 nanoparticles are uniform hollow spheres with inner cavities (Fig. 2(e) and Fig. ESI-1c†). With respect to size distributions (insets of Fig. ESI-1b and c†), the average diameters of AuNR@Nd_2O_3 composites and Nd_2O_3 hollow nanoparticles are similar, thus indicating that the iodide/triiodide electrolyte has not destroyed the Nd_2O_3 structure.[48] The extinction spectra obtained at different etching times are displayed in Fig. 2(f). The LSPR location is blue-shifted, and the intensity is systematically decreased. When AuNRs are completely etched, the absorption of AuNRs completely disappears. As shown in Fig. 2(g), the corresponding EDX spectrum also demonstrates that AuNRs have been etched thoroughly.

The plasmon-enhanced near-infrared luminescence of AuNR@Nd_2O_3 is further studied by comparing the composites' emission spectra before and after etching (Fig. 3(a)). For the measurement, a 730 nm continuous wave laser is used for excitation; the luminescence spectra are recorded by

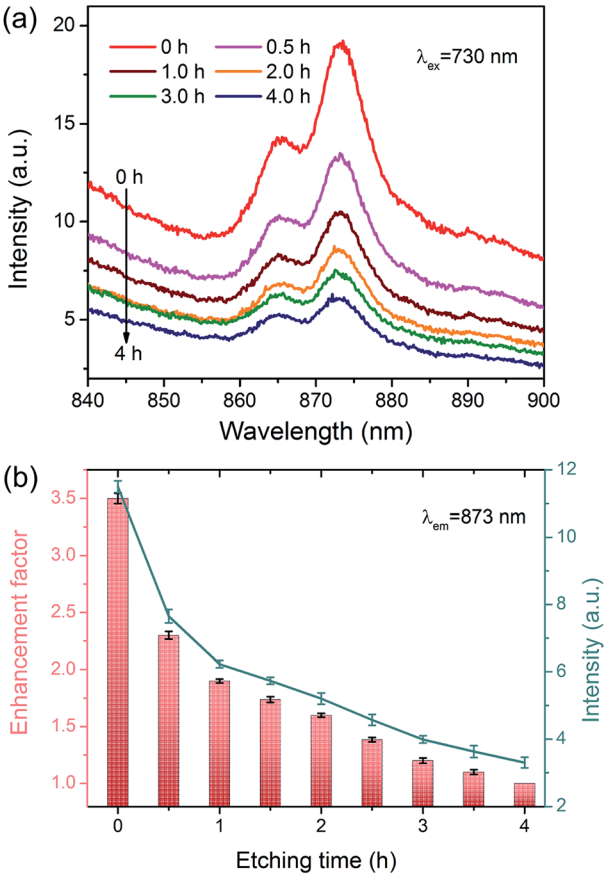

Fig. 3 (a) Emission spectra of AuNR@Nd_2O_3 composites during the etching process. (b) Emission enhancement factors and the emission intensities of 873 nm against the etching time.

a spectrometer with a liquid nitrogen-cooled CCD. The emission bands for the $^4F_{3/2}$–$^4I_{9/2}$ transition of Nd^{3+} are located at 873 nm. As AuNRs are corroded, the emission peak position and shape remain unchanged. To calculate the enhancement factors of 873 nm emission against the etching time, the emission spectra are decomposed by Gaussian fitting (Fig. ESI-2†); the emission intensities at 873 nm are displayed in Fig. 3(b). The corresponding enhancement factors are also calculated in Fig. 3(b); the largest enhancement of about 3.5 is obtained at the beginning. As the AuNRs are corroded, the emission intensity is decreased. In another words, the results suggest that as the Au content increases, the luminescence becomes brighter.

To further reveal the relationship between plasmon wavelength and luminescence enhancement, we prepared three kinds of AuNR@Nd_2O_3 with LSPRs at 740 nm (pink), 808 nm (green) and 880 nm (gray) (Fig. 4(a)). The emission spectra of the AuNR@Nd_2O_3 composites before and after etching were measured, and the enhancement factors at 873 nm emission are calculated in Fig. 4(b). The enhancement factors of Nd^{3+} at 873 nm were 4.6, 3.5 and 2.7 for the AuNR@Nd_2O_3 samples with LSPRs at 740 nm, 808 nm and 880 nm, respectively. When the LSPRs wavelength of AuNR@Nd_2O_3 is closer to the excitation wavelength, the enhancement factor was larger. The schematic of the plasmon-enhanced luminescence is shown in Fig. 5. Due

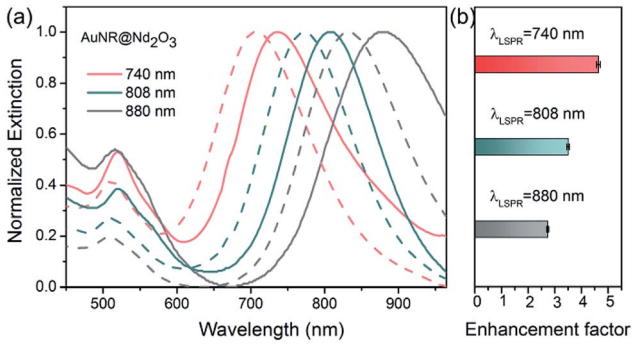

Fig. 4 (a) Extinction spectra of AuNR@Nd_2O_3 yolk/shell composites (solid lines) and the corresponding AuNRs (dashed lines) with different LSPRs. (b) Enhancement factors at 873 nm of AuNR@Nd_2O_3 with different LSPRs.

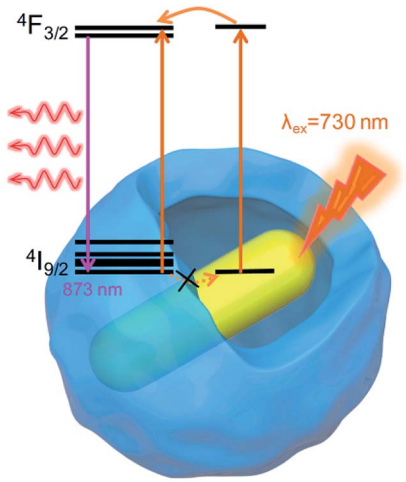

Fig. 5 Schematic mechanism of the energy transfer between an AuNR core and an Nd_2O_3 shell.

to the gap between AuNR and Nd_2O_3, the non-radiative energy transfer from Nd_2O_3 to AuNR was negligible (dashed arrows).[49] As the incident light excited AuNR and Nd_2O_3, the strong local electromagnetic field around AuNR enhanced the excitation and the emission processes of the Nd_2O_3 shells. There may be a resonance energy transfer between the AuNR and the Nd_2O_3, which was favorable for the improvement in Nd^{3+} excitation efficiency. As the LSPRs of AuNR@Nd_2O_3 were tuned from 740 nm to 880 nm, the enhancement factors decreased. All the results suggested that plasmons influenced the excitation process more efficiently than the emission process.

In summary, AuNR@Nd_2O_3 yolk/shell composites have been synthesized using a simple hydrothermal method. The reference samples (Nd_2O_3 hollow nanoparticles) are prepared by etching Au cores. The plasmon enhancement factor is also proved to be highly LSPR-dependent; the highest enhancement factor up to 4.6 is obtained when LSPR is resonant with the excitation. These findings provide a general pathway to modulate DCL of RE materials. The composites can be applied in photonics, bio-imaging, energy conversion and other fields.

Conflicts of interest

There are no conflicts to declare.

Acknowledgements

This work was jointly supported by the National Natural Science Foundation of China (51702352), China Postdoctoral Science Foundation (2017M612762), Shenzhen Science and Technology Research Funding (JCYJ20170307100227392).

Notes and references

1 H. Chen, Y. Lang, Y. Zhang, D. Zhao, G. Qin, C. Wu, K. Zheng and W. Qin, *J. Mater. Chem. C*, 2015, **3**, 6314–6321.
2 G. Tian, Z. Gu, X. Liu, L. Zhou, W. Yin, L. Yan, S. Jin, W. Ren, G. Xing, S. Li and Y. Zhao, *J. Phys. Chem. C*, 2011, **115**, 23790–23796.
3 T. Liu, Y. Wang, H. Qin, X. Bai, B. Dong, L. Sun and H. Song, *Mater. Res. Bull.*, 2011, **46**, 2296–2303.
4 X. Yu, L. Chen, M. Li, M. Xie, L. Zhou, Y. Li and Q. Wang, *Adv. Mater.*, 2008, **20**, 4118–4123.
5 G. S. Maciel and N. Rakov, *J. Mater. Chem. C*, 2013, **1**, 3563–3568.
6 M. Balestrieri, S. Colis, M. Gallart, G. Schmerber, M. Ziegler, P. Gilliot and A. Dinia, *J. Mater. Chem. C*, 2015, **3**, 7014–7021.
7 F. Liu, G. Aldea and J. Nunzi, *J. Lumin.*, 2010, **130**, 56–59.
8 X. Li, R. Wang, F. Zhang, L. Zhou, D. Shen, C. Yao and D. Zhao, *Sci. Rep.*, 2013, **3**, 3536.
9 T. Liu, Y. Wang, H. Qin, X. Bai, B. Dong, L. Sun and H. Song, *Mater. Res. Bull.*, 2011, **46**, 2296–2303.
10 C. Bouzigues, T. Gacoin and A. Alexandrou, *ACS Nano*, 2011, **5**, 8488–8505.
11 Z. A. Ansari, S. Khalid, A. A. Khan, H. Fouad and S. G. Ansari, *Sens. Lett.*, 2014, **12**, 1495–1501.
12 U. Rocha, K. U. Kumar, C. Jacinto, I. Villa, F. Sanz-Rodríguez, M. C. I. Cruz, A. Juarranz, E. Carrasco, F. C. J. M. Veggel, E. Bovero, J. G. Solé and D. Jaque, *Small*, 2014, **10**, 1141–1154.
13 C. Liu, Y. Hou and M. Gao, *Adv. Mater.*, 2014, **26**, 6922–6932.
14 Y. Li, P. Qiu, H. Duan, J. Chen, G. J. Snyder, X. Shi, B. B. Iversen and L. Chen, *J. Mater. Chem. C*, 2016, **4**, 4374–4379.
15 G. Jia, C. Zhang, S. Ding, L. Wang, L. Li and H. You, *CrystEngComm*, 2012, **14**, 573–578.
16 D. Yang, G. Li, X. Kang, Z. Cheng, P. a. Ma, C. Peng, H. Lian, C. Li and J. Lin, *Nanoscale*, 2012, **4**, 3450–3459.
17 H.-X. Mai, Y.-W. Zhang, L.-D. Sun and C.-H. Yan, *J. Phys. Chem. C*, 2007, **111**, 13721–13729.
18 H. Nabika and S. Deki, *J. Phys. Chem. B*, 2003, **107**, 9161–9164.
19 D. W. Lu, C. C. Mao, S. K. Cho, S. Ahn and W. Park, *Sci. Rep.*, 2016, **6**, 18894.
20 M. Fujii, T. Nakano, K. Imakita and S. Hayashi, *J. Phys. Chem. C*, 2013, **117**, 1113–1120.
21 Y. N. Xia and N. Halas, *MRS Bull.*, 2005, **30**, 338–348.

22 M. Rycenga, C. M. Cobley, J. Zeng, W. Y. Li, C. H. Moran, Q. Zhang, D. Qin and Y. N. Xia, *Chem. Rev.*, 2011, **111**, 3669–3712.
23 N. Li, H. Wang, M. Xue, C. Chang, Z. Chen, L. Zhou and B. Tang, *Chem. Commun.*, 2012, **48**, 2507–2509.
24 Z. Buch, V. Kumar, H. Mamgain and S. Chawla, *Chem. Commun.*, 2013, **49**, 9485–9487.
25 G. Kaur, R. K. Verma, D. K. Rai and S. B. Rai, *J. Lumin.*, 2012, **132**, 1683–1687.
26 J. Zhang, Y. Fu and J. R. Lakowicz, *J. Phys. Chem. C*, 2009, **113**, 19404–19410.
27 F. Zhang, G. B. Braun, Y. F. Shi, Y. C. Zhang, X. H. Sun, N. O. Reich, D. Y. Zhao and G. Stucky, *J. Am. Chem. Soc.*, 2010, **132**, 2850–2851.
28 A. Priyam, N. M. Idris and Y. Zhang, *J. Mater. Chem.*, 2012, **22**, 960–965.
29 M. Saboktakin, X. C. Ye, S. J. Oh, S. H. Hong, A. T. Fafarman, U. K. Chettiar, N. Engheta, C. B. Murray and C. R. Kagan, *ACS Nano*, 2012, **6**, 8758–8766.
30 P. Yuan, Y. H. Lee, M. K. Gnanasammandhan, Z. Guan, Y. Zhang and Q. Xu, *Nanoscale*, 2012, **4**, 5132–5137.
31 S. Lai, Z. Yang, J. Li, B. Shao, J. Yang, Y. Wang, J. Qiu and Z. Song, *J. Mater. Chem. C*, 2015, **3**, 7699–7708.
32 Y. Chen, K. Munechika and D. S. Ginger, *Nano Lett.*, 2007, **7**, 690–696.
33 Y. Bernhard, B. Collin and R. A. Decréau, *Sci. Rep.*, 2017, **7**, 45063.
34 H. Chen, L. Shao, Q. Li and J. Wang, *Chem. Soc. Rev.*, 2013, **42**, 2679–2724.
35 B. Reischl, A. L. Rohl, A. Kuronen and K. Nordlund, *Sci. Rep.*, 2017, **7**, 16257.
36 J. Shi, H. Wu, J. Liu, S. Li and X. He, *Sci. Rep.*, 2015, **5**, 11964.
37 J. Lu, M. Prabhu, J. Song, C. Li, J. Xu, K. Ueda, A. A. Kaminskii, H. Yagi and T. Yanagitani, *Appl. Phys. B*, 2000, **71**, 469–473.
38 B.-C. Ye and B.-C. Yin, *Angew. Chem., Int. Ed.*, 2008, **47**, 1–6.
39 R. Chhabra, J. Sharma, H. Wang, S. Zou, S. Lin, H. Yao, S. Lindsay and Y. Liu, *Nanotechnology*, 2009, **20**, 485201.
40 M. Chen, J. Wang, Z. Luo, Z. Cheng, Y. Zhang, X. Yu, L. Zhou and Q. Wang, *RSC Adv.*, 2016, **6**, 6912–6918.
41 T. Liu, X. Bai, C. Miao, Q. Dai, W. Xu, Y. Yu, Q. Chen and H. Song, *J. Phys. Chem. C*, 2014, **118**, 3258–3265.
42 J. Wang, H. Huang, D. Zhang, M. Chen, Y. Zhang, X. Yu, L. Zhou and Q. Wang, *Nano Res.*, 2015, **8**, 2548–2561.
43 B. Nikoobakht and M. A. El-Sayed, *Chem. Mater.*, 2003, **15**, 1957–1962.
44 N. R. Jana, L. Gearheart and C. J. Murphy, *Adv. Mater.*, 2001, **13**, 1389.
45 J. J. Mock, D. R. Smith and S. Schultz, *Nano Lett.*, 2003, **3**, 485–491.
46 N. Zhang, X. Fu and Y. Xu, *J. Mater. Chem.*, 2011, **21**, 8152–8158.
47 N. G. Bastús, J. Comenge and V. Puntes, *Langmuir*, 2011, **27**, 11098–11105.
48 C. H. Fang, H. L. Jia, S. Chang, Q. F. Ruan, P. Wang, T. Chen and J. F. Wang, *Energy Environ. Sci.*, 2014, **7**, 3431–3438.
49 C. D. Geddes and J. R. Lakowicz, *J. Fluoresc.*, 2002, **12**, 121–129.